GEOCHEMISTRY

Serpentinite-derived slab fluids control the oxidation state of the subarc mantle

Yuxiang Zhang[1,2,3]*, Esteban Gazel[4]*, Glenn A. Gaetani[5], Frieder Klein[6]

Recent geochemical evidence confirms the oxidized nature of arc magmas, but the underlying processes that regulate the redox state of the subarc mantle remain yet to be determined. We established a link between deep subduction-related fluids derived from dehydration of serpentinite ± altered oceanic crust (AOC) using B isotopes and B/Nb as fluid proxies, and the oxidized nature of arc magmas as indicated by Cu enrichment during magma evolution and V/Yb. Our results suggest that arc magmas derived from source regions influenced by a greater serpentinite (±AOC) fluid component record higher oxygen fugacity. The incorporation of this component into the subarc mantle is controlled by the subduction system's thermodynamic conditions and geometry. Our results suggest that the redox state of the subarc mantle is not homogeneous globally: Primitive arc magmas associated with flat, warm subduction are less oxidized overall than those generated in steep, cold subduction zones.

INTRODUCTION

The fugacity of oxygen (f_{O2}) in Earth's mantle fundamentally influences the generation and evolution of basaltic magmas (*1*). The overall higher f_{O2} recorded by arc magmas as compared to mid-ocean ridge basalts (MORB) has been widely attributed to the influence of oxidized slab materials on the magma sources (*2*, *3*), as evidenced by the positive correlations of f_{O2} with H_2O and fluid mobile element concentrations in arc and back-arc lavas (*4*, *5*). The redox budget of the subarc mantle also increases with subduction zone age and convergence rate (*6*, *7*). While these correlations are clear, a direct link between arc magma f_{O2} and the input of subducted oxidizing material is still lacking.

Altered oceanic crust (AOC) and sediments have long been considered as major subduction components involved in arc magma generation (*8*, *9*). However, the dehydration of subducted serpentinite has been increasingly recognized as an important source of volatiles (e.g., water, sulfur, and halogens) in the subarc mantle (*10*–*12*). Like AOC (*7*, *13*), breakdown of oxidized serpentinites can produce highly oxidizing fluids (*14*–*18*), which may have an important influence on the f_{O2} of arc magmas. Boron (B) isotopes ($\delta^{11}B = [(^{11}B/^{10}B)_{Sample}/(^{11}B/^{10}B)_{SRM951} - 1]*1000$) are a powerful tool for tracing the presence of serpentinite-derived fluids, as ^{11}B is depleted in the upper mantle [B < 0.1 parts per million (ppm); $\delta^{11}B = -10$ to -7‰] but is extremely enriched in serpentinite (up to 100 ppm B; $\delta^{11}B$ up to +40‰) (*19*). B/Nb is a second proxy for the subducted serpentinite, as this ratio is very high in serpentinite (up to 10^4) (*20*) and not strongly fractionated by magma differentiation processes (*21*). The positive correlation between $\delta^{11}B$ values and B/Nb for arc lavas is interpreted as reflecting the contributions of serpentinite fluid to the subarc mantle wedge (*22*, *23*).

To connect fluids derived from subducted serpentinite with the redox state of arc magmas, we investigated the relationships among $\delta^{11}B$ values and B/Nb with proxies for arc magma f_{O2} on a global scale. The abundance of Cu in arc magmas is controlled by saturation with sulfide, in which Cu is highly compatible (*24*). While sulfide saturation in silicate melt is influenced by pressure, temperature, melt composition, and H_2O concentration, f_{O2} is one of the most influential parameters (*25*–*28*). Sulfide (S^{2-}) is the dominant sulfur oxidation state at relatively low f_{O2} (e.g., < FMQ, fayalite-magnetite-quartz buffer), whereas at higher f_{O2}, the stable oxidation state of sulfur is S^{6+} (as sulfate). S^{6+} has up to 10 times greater solubility in magma than S^{2-} and the transition between the two sulfur species occurs within a narrow range of f_{O2} (e.g., FMQ to FMQ+2) (*25*, *26*). As a result, Cu shows contrasting behavior during magma evolution at different redox conditions: Cu enrichment due to suppression of sulfide saturation at high f_{O2}; Cu depletion due to sulfide segregation at low f_{O2} (Fig. 1) (*24*). Thus, Cu enrichments in the liquid lines of descent of arc magmas can be interpreted as reflecting high f_{O2} if the influences of other parameters can be excluded. In addition to Cu, we adopted V/Yb as a second proxy for f_{O2}. V is redox-sensitive whereas Yb is not, so that V/Yb fractionation varies as a function of oxygen fugacity during peridotite partial melting. That V and Yb are similarly incompatible during crystal fractionation means that this signal is not perturbed by shallow-level processes (*29*, *30*). V/Yb is also not sensitive to degree of mantle depletion (fig. S1).

RESULTS AND DISCUSSION

Cu behavior in arc magmas controlled by f_{O2}

The variation of Cu concentration during magmatic evolution of arc and back-arc lavas from three intraoceanic subduction zones (Mariana, Scotia, and Tonga) is shown in Fig. 1. The lavas from the back-arc basins generally have lower Cu concentrations than those in the corresponding arcs; there is a large data overlap between Tonga Arc and Lau Basin, partially due to the high Cu concentrations of primary Lau Basin magmas and/or the existence of immature spreading centers in the back-arc region. The trend of continuously decreasing Cu concentration with decreasing MgO concentration in the back-arc basins, indicative of early sulfide saturation, is

[1]Key Laboratory of Marine Geology and Environment, Institute of Oceanology, Chinese Academy of Sciences, Qingdao, Shandong, China. [2]Laboratory for Marine Mineral Resources, Qingdao Pilot National Laboratory for Marine Science and Technology, Qingdao, Shandong, China. [3]Center for Ocean Mega-Science, Chinese Academy of Sciences, Qingdao, Shandong, China. [4]Department of Earth and Atmospheric Sciences, Cornell University, Ithaca, NY, USA. [5]Department of Geology and Geophysics, Woods Hole Oceanographic Institution, Woods Hole, MA, USA. [6]Department of Marine Chemistry and Geochemistry, Woods Hole Oceanographic Institution, Woods Hole, MA, USA.
*Corresponding author. Email: zhangyuxiang13@mails.ucas.ac.cn (Y.Z.); egazel@cornell.edu (E.G.)

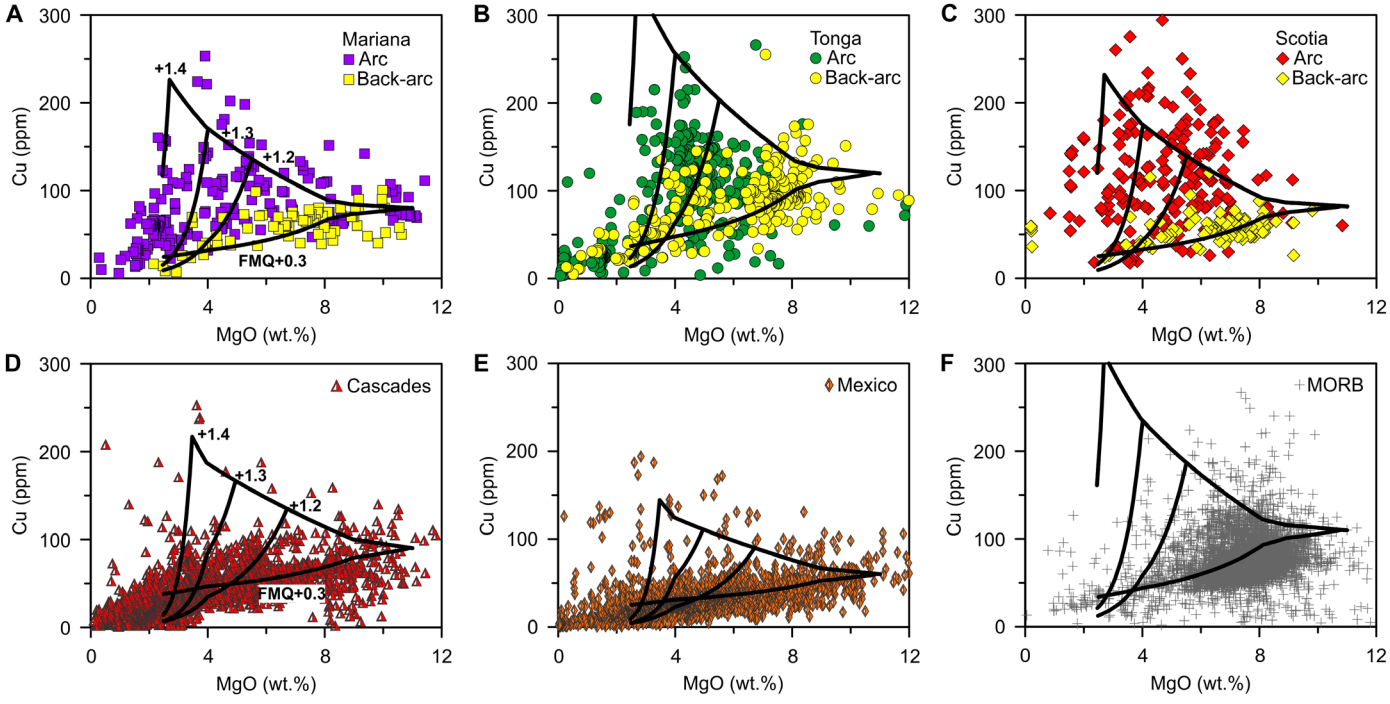

Fig. 1. Plots of Cu versus MgO for volcanic rocks from arcs and mid-ocean ridges. (**A** to **C**) Intraoceanic arcs, (**D** and **E**) Continental arcs, and (**F**) Mid-ocean ridges. Arc and back-arc data were plotted separately for the intraoceanic subduction zones. The black curves describe the behavior of Cu during magmatic differentiation at FMQ+0.3, +1.2, +1.3, and +1.4 following the models of (*24*). Tholeiitic differentiation model ($P = 0.2$ GPa) was used for intraoceanic arc lavas and MORB, and the Calc-alkaline differentiation model ($P = 0.8$ GPa) was used for continental arc lavas. The initial concentrations of S in the melt were set to be 1500 ppm.

markedly different from the trends observed in their arc counterparts, which show the highest concentration of Cu at 4 to 6 weight % (wt %) MgO (Fig. 1) but trends similar to those observed in thick continental arcs (crustal thickness > 30 km) (Fig. 1, D and E) and mid-ocean ridges (Fig. 1F).

Results from a previous study suggest that these distinct Cu evolution trends are controlled by arc crustal thickness. Thicker crust favors early magnetite crystallization, which induces sulfide saturation, whereas thinner crust retards magnetite crystallization, as indicated by the covariance of Cu and Fe concentrations for global arc lavas (*31*). Sulfide saturation in magma is also facilitated by high pressure (*27*). However, these models cannot explain the Cu depletion in lavas from back-arc basins and mid-ocean ridges, which are characterized by very thin crust. In addition, the concentrations of Cu and Fe_2O_{3T} (total Fe as Fe_2O_3) of the back-arc lavas do not follow a similar evolution trend (fig. S2). Other factors affecting sulfide saturation in magmas include sulfur concentration, temperature, and H_2O concentration (*26*, *28*). Magmas generated beneath mid-ocean ridges (perhaps including some back-arc basins) are generally characterized by lower sulfur concentrations (*32*) and higher temperatures (*33*) than arc magmas, which do not favor the observed early sulfide saturation (Fig. 1). Furthermore, the primary magmas from intraoceanic arcs and thick continental arcs share similar H_2O concentrations (*34*). Therefore, the parameters mentioned above cannot explain the systematic difference in the behaviors of sulfide saturation among intraoceanic arcs, thick continental arcs, back-arc basins, and mid-ocean ridges. We therefore attribute the saturation of sulfide in magmas to relatively reducing conditions, similar to MORB. The back-arc magmas are expected to have lower f_{O2} with increasing distance from the trench and, thus, weaker influence from subducted oxidized components as compared with arc magmas (*5*). For example, the lavas from the Mariana Trough record lower f_{O2} (FMQ+0.1 to FMQ+0.5) than those from the Mariana Arc (FMQ+1.0 to FMQ+1.6) (*4*). Using the method of (*24*), we modeled the behavior of Cu during magma differentiation at varying redox conditions. The results show that the magmas from back-arc basins, thick continental arcs, and mid-ocean ridges are mostly consistent with lower f_{O2} (~FMQ+0.3), while the magmas from intraoceanic arcs record higher f_{O2} (FMQ+1.2 to FMQ+1.4) (Fig. 1). This range of redox conditions overlaps with the f_{O2} associated with S^{2-}-S^{6+} transition (FMQ to FMQ+2) (*25*), meaning that the sulfur solubility in arc magmas is largely influenced by f_{O2}. The above indicates that high f_{O2} is a key factor leading to the Cu enrichment during arc magma evolution.

Cu enrichment during arc magma evolution promoted by ^{11}B-rich slab fluids

We found that the lavas from intraoceanic arcs that show Cu enrichment during magma evolution are characterized by heavy B isotopes (fig. S3). The heavy B isotopes in the lavas from the Mariana Arc ($\delta^{11}B_{aver.} \approx +4.5‰$), Tonga Arc ($\delta^{11}B_{aver.} \approx +8.3‰$), and South Sandwich Arc ($\delta^{11}B_{aver.} \approx +15.0‰$) cannot be explained by the contribution of fluids from the subducted sediments ($\delta^{11}B$ mostly negative) (*35*). AOC typically has low to moderate $\delta^{11}B$ values (mostly 0 to +5‰); the AOC metamorphosed at high temperatures can be characterized by heavy B isotopes ($\delta^{11}B$ up to > +10‰) (*19*, *36*). Despite the high $\delta^{11}B$ values, subducting AOC preferentially loses ^{11}B during dehydration and, thereby, will probably have low

$\delta^{11}B$ at subarc depths (*22*, *23*). In comparison, subducted serpentinite can retain heavy B isotopes ($\delta^{11}B$ up to +34‰) until serpentine minerals break down at depths down to >200 km (*11*, *37*), making it the most likely major source of isotopically heavy B in arc magmas (*22*, *23*, *38*, *39*). B isotopes in arc lavas tend to become progressively lighter with distance behind the trench (fig. S3). The back-arc basin lavas, which have little or no Cu enrichment with decreasing MgO, have much lighter B isotopes than the arc lavas (fig. S3), for example, Mariana Trough ($\delta^{11}B_{aver.} \approx -4.7$‰, as compared to +4.5‰ of Mariana Arc) and Lau Basin ($\delta^{11}B_{aver.} \approx -2$‰, as compared to +8.3‰ of Tonga Arc), suggesting the limited participation of serpentinite-derived fluids in the back-arc mantle.

We investigated the relationships of Cu enrichment during arc magma evolution to B isotopes and B/Nb using a global arc dataset (including some back-arc basin data) (Fig. 2, A and B). Here, we used the relative Cu enrichment at 4 to 6 wt % MgO [$\Delta Cu_{(4-6)} = Cu_{(4-6)}/Cu_{(8-12)} - 1$, where $Cu_{(4-6)}$ and $Cu_{(8-12)}$ are the concentrations Cu in arc lavas containing 4 to 6 wt % and 8 to 12 wt % MgO, respectively] to evaluate Cu enrichment or depletion for each arc; although this MgO range cannot represent primitive arc magmas, $\Delta Cu_{(4-6)}$ values show whether sulfide saturation is reached at an early stage of magma evolution and, thus, might indicate primitive magma f_{O2}. While magma f_{O2} can increase during differentiation, i.e., via the fractionation of Fe(II)-rich minerals (such as almandine), such an effect is small during basaltic to andesitic differentiation (*40*). It is noted that the intermediate lavas can also be produced by mixing of mafic and felsic magmas. However, the mixing scenario is not consistent with the higher Cu concentrations of intermediate magmas in many arcs, as both the mafic and felsic lavas are depleted in Cu (Fig. 1) (*24*, *31*).

The average B isotopic compositions and B/Nb are plotted against $\Delta Cu_{(4-6)}$ values for the lavas from 12 Pliocene-Quaternary aged arcs and two back-arc basins (see Materials and Methods for the calculations of averages) (Fig. 2, A and B). We found that the $\Delta Cu_{(4-6)}$ values show significant positive correlations with the B isotopes ($r^2 = 0.74$) and B/Nb ($r^2 = 0.79$) for the global arc dataset. Similar relationships are observed between $Cu_{(4-6)}$ values and $\delta^{11}B$, B/Nb (fig. S4, A and B). Although we cannot exclude the influences of AOC-derived fluids on the arcs with low to moderate $\delta^{11}B$ values, these correlations indicate that a strong relationship exists between Cu enrichment during arc magma evolution and subducted serpentinite fluids carrying heavy B. $\Delta Cu_{(4-6)}$ values are not affected by Cu enrichment or depletion in the magma source. Thus, we suggest that the above correlations reflect the role of serpentinite-derived fluids in controlling the behavior of Cu in the melt by influencing the f_{O2} of the system and, thus, the state of sulfide saturation. This interpretation is also supported by the positive correlations of the average V/Yb of primitive arc lavas [8 to 12 wt % MgO; $V/Yb_{(8-12)}$], a proxy for f_{O2} (*29*, *30*), with the average $\delta^{11}B$ values ($r^2 = 0.77$) and average B/Nb ($r^2 = 0.84$) for our global arc dataset (Fig. 2, C and D).

Serpentinite can recycle substantial amounts of H_2O, sulfur (as HSO_4^- or SO_4^{2-}), and carbon into the upper mantle at convergent margins (*10*, *11*, *16*). Of particular interest is that sulfate (S^{6+}) has strong oxidizing capacity when it is reduced to sulfide (S^{2-}) (*5*). In addition, H_2O concentrations correlate with the Fe(III)/ΣFe in the melt and, while H_2O itself is generally not considered to be an oxidizing agent, this correlation suggests that slab-derived fluids are involved in the redox reactions (*6*); results from a recent study do, however, suggest the possibility that hydrous melts can be oxidized by H_2O dissociation and hydrogen incorporation into orthopyroxene (*41*). Furthermore, ~$^2/_3$ of the Fe in serpentinite is ferric, which is hosted by magnetite and serpentine minerals (lizardite, chrysotile, and antigorite). Previous studies suggested that the Fe(III)/ΣFe decreases during metamorphism and deserpentinization (*14*). This inference rests on the assumption that the protoliths of variably metamorphosed serpentinites had a consistent Fe(III)/ΣFe to begin with, which, however, cannot be unequivocally determined (*18*). If metamorphism and deserpentinization does result in a decrease of Fe(III)/ΣFe, the reduction of Fe(III) to Fe(II) would require the formation of an oxidized component such as SO_x or CO_x. This interpretation, while still debated, would suggest that serpentinite dehydration has the potential to release oxidizing fluids with an isotopically heavy $\delta^{11}B$ signature (*15*–*17*, *23*).

Evans and Frost (*18*) elaborated on a variety of processes that may affect the redox budget of subducted serpentinites and, thereby, the capacity of serpentinite-derived fluids to oxidize subarc mantle. While some studies conclude that fluids released by serpentine dehydration are sufficiently oxidized to affect the redox budget of arc magmas (*15*–*17*), others suggest that these fluids may be notably less oxidized (*42*). Serpentinite within the subducting plate has isotopically heavy B ($\delta^{11}B$ up to +40‰) and is a possible source of ^{11}B in arc magmas (*37*). However, the modern subducting plates are mostly generated at fast-spreading ridges, where the interactions between lithospheric mantle and fluids are relatively limited, and thus, it is questionable whether such serpentinites are as oxidized as those formed at slow-spreading ridges (*18*). In comparison, forearc serpentinite, extensively metasomatized by sulfate-bearing fluids released from subducting slab at shallow depth (*43*), is probably more oxidized and also has relatively heavy B isotopes ($\delta^{11}B$ up to +15‰) (*44*). However, it is debatable whether the serpentinized forearc mantle is transported to the subarc depth by the subducting slab or corner flow (*20*, *45*). Therefore, based on the current knowledge, it is not possible to determine which kind of serpentinite is the major fluid source. Despite these uncertainties, the robust correlations between magma f_{O2} proxies and $\delta^{11}B$ values for global arcs favor the conclusion that serpentinite-derived fluids play an important role in establishing the redox conditions in the subarc mantle. Here, again, we cannot exclude the influence of AOC-derived fluids, which are also recognized to be oxidizing (*7*, *13*). It is likely that the redox state of subarc mantle is influenced by a combination of AOC- and serpentinite-derived fluids, which may form a high $\delta^{11}B$ and oxidizing composite slab fluid.

Implications for the f_{O2} of primitive arc magmas

Dehydration of serpentine minerals is controlled by the pressure-temperature conditions of the subduction system (fig. S5) and the thermal structure of subduction zone varies with slab age and dip (*46*). Multivariate analysis shows that subducting slab dip significantly correlates with the amount of ^{11}B-rich, oxidizing serpentinite fluids that lastly reach the subarc mantle (table S1). Shallow slabs are generally associated with warm subduction (fig. S5C) and the higher temperatures will lead to shallow dehydration of serpentinite (fig. S5, A and B), thereby depleting the slab with respect to ^{11}B at subarc depth. These slabs usually have low descent rates and longer arc-trench distances and, thus, reside beneath the mantle wedge for much longer times and dehydrate more efficiently (fig. S5, D and E) (*22*). The slab dip is likely the main control on the mechanisms of

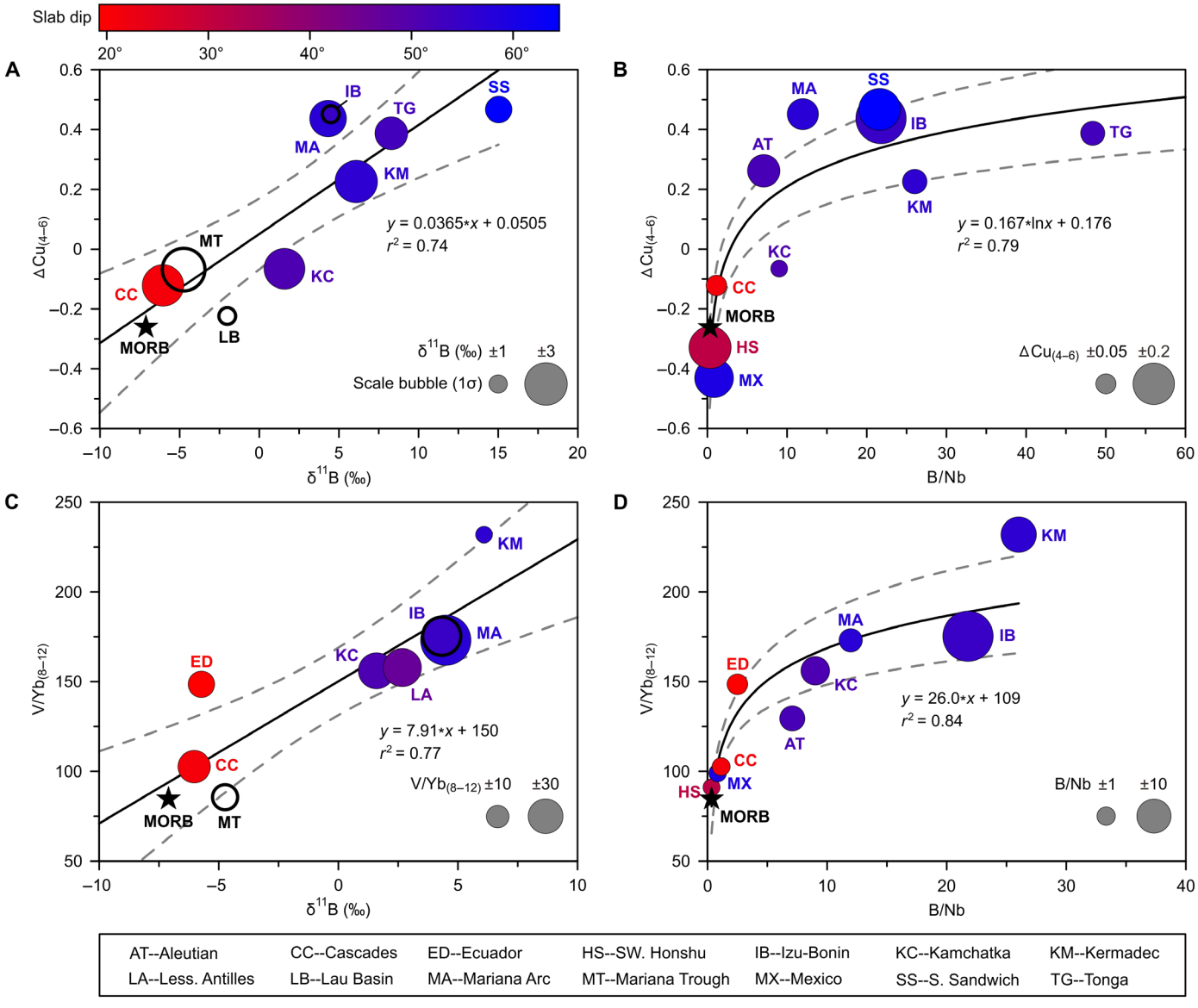

Fig. 2. Bubble plots showing the correlations of magma f_{O2} proxies with slab fluid proxies for global arcs. (**A**) $\Delta Cu_{(4-6)}$ versus $\delta^{11}B$, (**B**) $\Delta Cu_{(4-6)}$ versus B/Nb, (**C**) $V/Yb_{(8-12)}$ versus $\delta^{11}B$, and (**D**) $V/Yb_{(8-12)}$ versus B/Nb. Each point represents the average values of $\delta^{11}B$, B/Nb, $\Delta Cu_{(4-6)}$, or $V/Yb_{(8-12)}$ for each individual arc segment and MORB (table S2). The bubble color indicates the slab dip and the bubble radius is proportional to 1σ uncertainties of the variable [$\delta^{11}B$, $\Delta Cu_{(4-6)}$, V/Yb, and B/Nb]. See Materials and Methods for more details about how the average values are obtained.

slab fluids delivery into the mantle wedge; fluid flux from a steep slab will be focused beneath the arc and, thus, deeper fluids from the breakdown of subducted serpentinite have a higher potential for becoming an important contribution to arc magmas (Fig. 3) (*47*). Consequently, arc lavas from steep subduction zones are probably influenced by more recycled serpentinite fluids and thereby have higher $\delta^{11}B$, B/Nb, $\Delta Cu_{(4-6)}$ values, and $V/Yb_{(8-12)}$ compared to those from flat subduction (Fig. 2). One exception is the Mexican Arc, where the slab beneath the arc markedly changed from shallow dip to a very steep angle at ~7 Ma (million years), and there are also complexities with an OIB-like source sampled by these volcanoes (*48*). The extremely heavy B isotopes observed in the South Sandwich Arc lavas may be partly due to the subduction erosion of serpentinized forearc mantle (*39*) or the subduction of serpentinized mantle near the seafloor formed by slow-spreading tectonics of the South Atlantic (*49*).

In summary, a combination of the thermal structure and geometry of the subduction zone provides a first-order control on the incorporation of ^{11}B-rich, oxidizing fluid derived from deserpentinization into the source regions of arc magmas. Results from thermodynamic models suggest that AOC dehydration produces oxidizing fluids more efficiently in cold subduction than in warm subduction (*13*). These results imply that the average f_{O2} of subarc mantle is not homogeneous globally. Some thick continental arcs in the eastern Pacific (e.g., Ecuador, Mexico, and Cascades) are generally characterized by shallow, hot/warm subduction, which would result

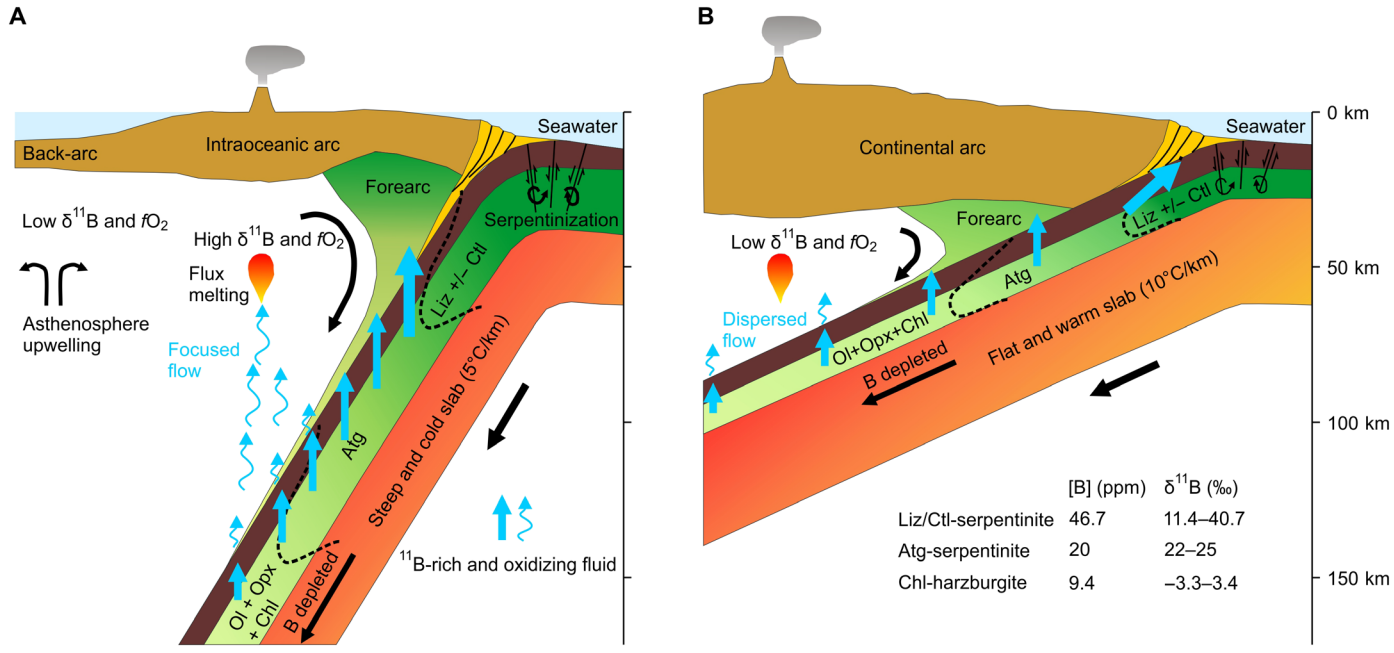

Fig. 3. Sketch of serpentinite subduction [modified after (*12*)]. (**A**) Steep, cold subduction zone and (**B**) Flat, warm subduction zone. Dehydration of serpentine minerals [lizardite (Liz), chrysotile (Ctl), and antigorite (Atg)] releases ^{11}B-rich and oxidizing fluids. The migration of such fluids into the subarc mantle is promoted by steep, cold subduction, but is limited by flat, warm subduction. The depths of lizardite ± chrysotile to antigorite transition (200 to 400°C) (*12*) and antigorite breakdown (600 to 700°C) (*61*) are determined according to a thermal gradient of 5°C/km for cold subduction and 10°C/km for warm subduction (*62*). The B concentrations and δ^{11}B of serpentinite and chlorite (Chl) harzburgite are from (*37*, *63*).

in light δ^{11}B values, similar to those of MORB mantle; based on the Cu depletion and low V/Yb (Figs. 1 and 2), the primary magmas in these arcs will generally have lower f_{O2} due to the lack of contributions from an oxidizing fluid. Conversely, the subarc mantle of some intraoceanic arcs with steep and/or cold subducting plates (e.g., Mariana, Tonga, and Izu-Bonin) are expected to be overall more oxidized and, therefore, to generate sulfide-undersaturated magma. Results from a previous study suggest that the redox states of global primitive arc lavas and MORB are indistinguishable as indicated by their similar Cu concentrations (*24*). However, our results show that the Cu concentrations of primitive arc lavas (MgO = 8 to 12 wt %) are not identical globally and they also show positive correlations with δ^{11}B and B/Nb, but they are not higher than the Cu concentrations of primitive back-arc lavas and MORB (fig. S4, C and D). The Cu concentrations of mantle partial melt are controlled by many factors, in addition to f_{O2}, such as extent of partial melting, Cu concentrations of mantle sources (*24*), etc.; thus, they are probably not robust proxies for the mantle f_{O2}.

Our conclusions are based on the average estimates for entire arc segments. The f_{O2} can be highly heterogeneous within a single arc (e.g., from FMQ to FMQ+2) (*50*). High f_{O2} lavas (e.g., ~FMQ+2) have been observed in some continental arcs, such as Mexico (*3*) and Cascades (*51*). Sporadic Cu enrichment also occurs in these arcs (Fig. 1, D and E). This may reflect the roles of multisourced subduction input, intracrustal processes (e.g., crustal contamination and deep crystallization), and/or mantle heterogeneity in the formation of chemically diverse arc volcanic rocks (*52*). Despite this, the significant global correlations among δ^{11}B, B/Nb, $\Delta Cu_{(4-6)}$ values, and V/Yb denote that independent of local heterogeneity, recycling of oxidizing slab fluids probably have an important control on the oxidation state of subarc mantle.

MATERIALS AND METHODS

Data compilation and filtration

The data of Cu, MgO, Fe_2O_{3T}, δ^{11}B, B, Nb, V, and Yb for the lavas from 16 Pliocene-Quaternary aged arcs and three back-arc basins (Mariana Trough, Lau Basin, and East Scotia Ridge) used in this study are from the GEOROC database (http://georoc.mpch-mainz.gwdg.de/georoc/). Some δ^{11}B and B/Nb data are from literature (*38*, *39*, *53*–*57*). The MORB data are from the PetDB database (www.earthchem.org/petdb/). These data include whole-rock or glass compositions of volcanic rocks. Melt inclusion data were also included for δ^{11}B and B/Nb. Boninites were not considered here as they are products of subduction initiation and exist in only a few arcs. The samples that are described as altered or have LOI higher than 2 wt % were discarded from the dataset. All outliers were cross-checked with the original publications. The northern part of the Lau Basin and Tonga Arc is influenced by mantle plume (*58*), and, thus, only the data to the south of 17°S were used. Note that Fonualei Spreading Center was divided into the Tonga Arc for the lava show arc signature (*59*). All the data mentioned above are given in data S1.

As B isotope fractionation during the magma differentiation is insignificant (*19*), the δ^{11}B data were not filtered according to MgO concentrations. B/Nb is also little influenced by magma differentiation (*21*). However, the B/Nb ratio shows large variations at MgO < 2 wt % for some arcs (fig. S6); thus, the data for MgO < 2 wt % were removed. We note that crustal contamination can substantially

influence the B isotopes and B/Nb of magmas; thus, we have gone back to the original publications and removed the data affected by crustal contamination. The V/Yb of the arc lavas shows sharp decrease with the decreasing MgO concentrations at MgO < 6 wt % (fig. S7). We used the data at MgO = 8 to 12 wt % to represent the compositions of primitive arc magma. This MgO range can minimize the effect of magnetite crystallization on V contents. We also removed the data with Dy/Yb > 2 to exclude the effects of residual garnet in the source (*29*). It is shown whether arc lavas are enriched or depleted in Cu at 4 to 6 wt % MgO (*31*); thus, we used the relative Cu enrichment at 4 to 6 wt % MgO [$\Delta Cu_{(4-6)} = Cu_{(4-6)}/Cu_{(8-12)} - 1$, where $Cu_{(4-6)}$ and $Cu_{(8-12)}$ indicate Cu concentrations at MgO = 4 to 6 wt % and 8 to 12 wt %, respectively] to evaluate Cu enrichment or depletion for each arc.

Determination of average values for each arc segment

The averages of $\delta^{11}B$ value, B/Nb, Cu concentration at MgO = 4 to 6 wt % [$Cu_{(4-6)}$] and 8 to 12 wt % [$Cu_{(8-12)}$], and V/Yb at MgO = 8–12 wt % [$V/Yb_{(8-12)}$] were calculated for each individual arc. To reduce the sampling bias toward certain volcanoes and to get a reliable estimation of arc averages, the filtered data were first averaged within volcanoes (or volcanic zones) and then averaged within arc segments, following the method of (*60*). For Cu concentrations and V/Yb, at least two data points were required for determining the volcano averages; for $\delta^{11}B$ and B/Nb, one data point was allowed to represent a volcano. At least two volcanoes were required for the calculation of arc averages. The back-arc averages were obtained by averaging all the samples. The MORB averages were calculated following the method of (*31*): The data were firstly subgrouped (at intervals ≥0.5 wt %) and median values were calculated for each subgroup; then, the average values and 1σ uncertainties were calculated from the median values. This method can reduce the bias caused by outliers.

The average values for arc segment and each volcano are given in table S2 and data S1, respectively. The calculated $Cu_{(4-6)}$ values for each arc are overall consistent with those obtained by averaging all the samples (fig. S8A) (*31*). The locations of the volcanoes with available data of $\delta^{11}B$, B/Nb, Cu concentrations, and V/Yb are shown in figs. S9 to S13. The distributions of B isotope data by volcanoes for each arc are shown in fig. S14. Although the available B isotope and B/Nb data are relatively in small quantity, they mostly cover a large part of the arcs. The arc average Cu concentration and V/Yb obtained by all the volcanoes are consistent with those obtained by the volcanoes with available $\delta^{11}B$ or B/Nb (fig. S8, B and C). Thus, we believe that the observed $\delta^{11}B$ or B/Nb can be representative of the values of the whole arc segment.

SUPPLEMENTARY MATERIALS

Supplementary material for this article is available at https://science.org/doi/10.1126/sciadv.abj2515

REFERENCES AND NOTES

1. D. J. Frost, C. A. McCammon, The redox state of Earth's mantle. *Annu. Rev. Earth Planet. Sci.* **36**, 389–420 (2008).
2. C. Ballhaus, R. F. Berry, D. H. Green, Oxygen fugacity controls in the Earth's upper mantle. *Nature* **348**, 437–440 (1990).
3. I. S. E. Carmichael, The redox states of basic and silicic magmas: A reflection of their source regions? *Contrib. Mineral. Petrol.* **106**, 129–141 (1991).
4. M. N. Brounce, K. A. Kelley, E. Cottrell, Variations in $Fe^{3+}/\sum Fe$ of Mariana arc basalts and mantle wedge fO_2. *J. Petrol.* **55**, 2513–2536 (2014).
5. K. A. Kelley, E. Cottrell, Water and the oxidation state of subduction zone magmas. *Science* **325**, 605–607 (2009).
6. K. A. Evans, M. A. Elburg, V. S. Kamenetsky, Oxidation state of subarc mantle. *Geology* **40**, 783–786 (2012).
7. M. Brounce, E. Cottrell, K. A. Kelley, The redox budget of the Mariana subduction zone. *Earth Planet. Sci. Lett.* **528**, 115859 (2019).
8. C. Chauvel, E. Lewin, M. Carpentier, N. T. Arndt, J.-C. Marini, Role of recycled oceanic basalt and sediment in generating the Hf–Nd mantle array. *Nat. Geosci.* **1**, 64–67 (2008).
9. T. Plank, C. H. Langmuir, Tracing trace elements from sediment input to volcanic output at subduction zones. *Nature* **362**, 739–743 (1993).
10. J. C. Alt, C. J. Garrido, W. C. Shanks III, A. Turchyn, J. A. Padrón-Navarta, V. L. Sánchez-Vizcaíno, M. T. G. Pugnaire, C. Marchesi, Recycling of water, carbon, and sulfur during subduction of serpentinites: A stable isotope study of Cerro del Almirez, Spain. *Earth Planet. Sci. Lett.* **327–328**, 50–60 (2012).
11. L. H. Rüpke, J. P. Morgan, M. Hort, J. A. D. Connolly, Serpentine and the subduction zone water cycle. *Earth Planet. Sci. Lett.* **223**, 17–34 (2004).
12. L. Pagé, K. Hattori, Abyssal serpentinites: Transporting halogens from Earth's surface to the deep mantle. *Minerals* **9**, 61 (2019).
13. J. B. Walters, A. M. Cruz-Uribe, H. R. Marschall, Sulfur loss from subducted altered oceanic crust and implications for mantle oxidation. *Geochem. Perspect. Lett.* **13**, 36–41 (2020).
14. B. Debret, N. Bolfan-Casanova, J. A. Padrón-Navarta, F. Martin-Hernandez, M. Andreani, C. J. Garrido, V. López Sánchez-Vizcaíno, M. T. Gómez-Pugnaire, M. Muñoz, N. Trcera, Redox state of iron during high-pressure serpentinite dehydration. *Contrib. Mineral. Petrol.* **169**, 36 (2015).
15. K. Iacovino, M. R. Guild, C. B. Till, Aqueous fluids are effective oxidizing agents of the mantle in subduction zones. *Contrib. Mineral. Petrol.* **175**, 36 (2020).
16. B. Debret, D. A. Sverjensky, Highly oxidising fluids generated during serpentinite breakdown in subduction zones. *Sci. Rep.* **7**, 10351 (2017).
17. J. Maurice, N. Bolfan-Casanova, S. Demouchy, P. Chauvigne, F. Schiavi, B. Debret, The intrinsic nature of antigorite breakdown at 3 GPa: Experimental constraints on redox conditions of serpentinite dehydration in subduction zones. *Contrib. Mineral. Petrol.* **175**, 94 (2020).
18. K. A. Evans, B. R. Frost, Deserpentinization in subduction zones as a source of oxidation in arcs: A reality check. *J. Petrol.* **62**, egab016 (2021).
19. H. R. Marschall, Boron isotopes in the ocean floor realm and the mantle, in *Boron Isotopes: The Fifth Element*, H. Marschall, G. Foster, Eds. (Springer, Cham, 2018), pp. 189–215.
20. I. P. Savov, J. G. Ryan, M. D'Antonio, P. Fryer, Shallow slab fluid release across and along the Mariana arc-basin system: Insights from geochemistry of serpentinized peridotites from the Mariana fore arc. *J. Geophys. Res. Solid Earth* **112**, B09205 (2007).
21. J. G. Ryan, W. P. Leeman, J. D. Morris, C. H. Langmuir, The boron systematics of intraplate lavas: Implications for crust and mantle evolution. *Geochim. Cosmochim. Acta* **60**, 415–422 (1996).
22. J. C. M. De Hoog, I. P. Savov, Boron isotopes as a tracer of subduction zone processes, in *Boron Isotopes: The Fifth Element*, H. Marschall, G. Foster, Eds. (Springer, Cham, 2018), pp. 217–247.
23. M. Scambelluri, S. Tonarini, Boron isotope evidence for shallow fluid transfer across subduction zones by serpentinized mantle. *Geology* **40**, 907–910 (2012).
24. C.-T. A. Lee, P. Luffi, E. J. Chin, R. Bouchet, R. Dasgupta, D. M. Morton, V. le Roux, Q. Z. Yin, D. Jin, Copper systematics in arc magmas and implications for crust-mantle differentiation. *Science* **336**, 64–68 (2012).
25. P. J. Jugo, R. W. Luth, J. P. Richards, Experimental data on the speciation of sulfur as a function of oxygen fugacity in basaltic melts. *Geochim. Cosmochim. Acta* **69**, 497–503 (2005).
26. W. M. Nash, D. J. Smythe, B. J. Wood, Compositional and temperature effects on sulfur speciation and solubility in silicate melts. *Earth Planet. Sci. Lett.* **507**, 187–198 (2019).
27. J. A. Mavrogenes, H. S. C. O'Neill, The relative effects of pressure, temperature and oxygen fugacity on the solubility of sulfide in mafic magmas. *Geochim. Cosmochim. Acta* **63**, 1173–1180 (1999).
28. M.-A. Fortin, J. Riddle, Y. Desjardins-Langlais, D. R. Baker, The effect of water on the sulfur concentration at sulfide saturation (SCSS) in natural melts. *Geochim. Cosmochim. Acta* **160**, 100–116 (2015).
29. M. Laubier, T. L. Grove, C. H. Langmuir, Trace element mineral/melt partitioning for basaltic and basaltic andesitic melts: An experimental and laser ICP-MS study with application to the oxidation state of mantle source regions. *Earth Planet. Sci. Lett.* **392**, 265–278 (2014).
30. G. Mallmann, H. S. C. O'Neill, The crystal/melt partitioning of V during mantle melting as a function of oxygen fugacity compared with some other elements (Al, P, Ca, Sc, Ti, Cr, Fe, Ga, Y, Zr and Nb). *J. Petrol.* **50**, 1765–1794 (2009).
31. M. Chiaradia, Copper enrichment in arc magmas controlled by overriding plate thickness. *Nat. Geosci.* **7**, 43–46 (2014).

32. P. J. Wallace, M. Edmonds, The sulfur budget in magmas: Evidence from melt inclusions, submarine glasses, and volcanic gas emissions. *Rev. Mineral. Geochem.* **73**, 215–246 (2011).
33. C.-T. A. Lee, P. Luffi, T. Plank, H. Dalton, W. P. Leeman, Constraints on the depths and temperatures of basaltic magma generation on Earth and other terrestrial planets using new thermobarometers for mafic magmas. *Earth Planet. Sci. Lett.* **279**, 20–33 (2009).
34. T. Plank, K. A. Kelley, M. M. Zimmer, E. H. Hauri, P. J. Wallace, Why do mafic arc magmas contain ~4wt% water on average? *Earth Planet. Sci. Lett.* **364**, 168–179 (2013).
35. T. Ishikawa, E. Nakamura, Boron isotope systematics of marine sediments. *Earth Planet. Sci. Lett.* **117**, 567–580 (1993).
36. A. M. McCaig, S. S. Titarenko, I. P. Savov, R. A. Cliff, D. Banks, A. Boyce, S. Agostini, No significant boron in the hydrated mantle of most subducting slabs. *Nat. Commun.* **9**, 4602 (2018).
37. J. Harvey, C. J. Garrido, I. Savov, S. Agostini, J. A. Padrón-Navarta, C. Marchesi, V. López Sánchez-Vizcaíno, M. T. Gómez-Pugnaire, ^{11}B-rich fluids in subduction zones: The role of antigorite dehydration in subducting slabs and boron isotope heterogeneity in the mantle. *Chem. Geol.* **376**, 20–30 (2014).
38. W. P. Leeman, S. Tonarini, S. Turner, Boron isotope variations inTonga-Kermadec-NewZealand arc lavas: Implications for the origin of subduction components and mantle influences. *Geochem. Geophys. Geosyst.* **18**, 1126–1162 (2017).
39. S. Tonarini, W. P. Leeman, P. T. Leat, Subduction erosion of forearc mantle wedge implicated in the genesis of the South Sandwich Island (SSI) arc: Evidence from boron isotope systematics. *Earth Planet. Sci. Lett.* **301**, 275–284 (2011).
40. M. Tang, C.-T. A. Lee, G. Costin, H. E. Höfer, Recycling reduced iron at the base of magmatic orogens. *Earth Planet. Sci. Lett.* **528**, 115827 (2019).
41. P. Tollan, J. Hermann, Arc magmas oxidised by water dissociation and hydrogen incorporation in orthopyroxene. *Nat. Geosci.* **12**, 667–671 (2019).
42. F. Piccoli, J. Hermann, T. Pettke, J. A. D. Connolly, E. D. Kempf, J. F. Vieira Duarte, Subducting serpentinites release reduced, not oxidized, aqueous fluids. *Sci. Rep.* **9**, 19573 (2019).
43. J. Alt, W. Shanks III, Stable isotope compositions of serpentinite seamounts in the Mariana forearc: Serpentinization processes, fluid sources and sulfur metasomatism. *Earth Planet. Sci. Lett.* **242**, 272–285 (2006).
44. L. D. Benton, J. G. Ryan, F. Tera, Boron isotope systematics of slab fluids as inferred from a serpentine seamount, Mariana forearc. *Earth Planet. Sci. Lett.* **187**, 273–282 (2001).
45. I. Wada, K. Wang, J. He, R. D. Hyndman, Weakening of the subduction interface and its effects on surface heat flow, slab dehydration, and mantle wedge serpentinization. *J. Geophys. Res. Solid Earth* **113**, B04402 (2008).
46. E. M. Syracuse, P. E. van Keken, G. A. Abers, The global range of subduction zone thermal models. *Phys. Earth Planet. Inter.* **183**, 73–90 (2010).
47. C. R. Wilson, M. Spiegelman, P. E. van Keken, B. R. Hacker, Fluid flow in subduction zones: The role of solid rheology and compaction pressure. *Earth Planet. Sci. Lett.* **401**, 261–274 (2014).
48. L. Ferrari, T. Orozco-Esquivel, V. Manea, M. Manea, The dynamic history of the Trans-Mexican Volcanic Belt and the Mexico subduction zone. *Tectonophysics* **522-523**, 122–149 (2012).
49. T. Plank, C. E. Manning, Subducting carbon. *Nature* **574**, 343–352 (2019).
50. E. Cottrell, S. Birner, M. Brounce, F. Davis, L. Waters, K. Kelley, Oxygen fugacity across tectonic settings. *Earth Space Sci. Open Arch.* 10.1002/essoar.10502445.1 (2020).
51. M. Muth, P. J. Wallace, G. A. Gaetani, paper presented at the AGU Fall Meeting, San Francisco, CA, 9–13 December 2019.
52. W. P. Leeman, Old/new subduction zone paradigms as seen from the cascades. *Front. Earth Sci.* **8**, 535879 (2020).
53. G. F. Cooper, C. G. Macpherson, J. D. Blundy, B. Maunder, R. W. Allen, S. Goes, J. S. Collier, L. Bie, N. Harmon, S. P. Hicks, A. A. Iveson, J. Prytulak, A. Rietbrock, C. A. Rychert, J. P. Davidson; the VoiLA team, G. F. Cooper, C. G. Macpherson, J. D. Blundy, B. Maunder, R. W. Allen, S. Goes, J. S. Collier, L. Bie, N. Harmon, S. P. Hicks, A. Rietbrock, C. A. Rychert, J. P. Davidson, R. G. Davy, T. J. Henstock, M. J. Kendall, D. Schlaphorst, J. van Hunen, J. J. Wilkinson, M. Wilson, Variable water input controls evolution of the Lesser Antilles volcanic arc. *Nature* **582**, 525–529 (2020).
54. T. Ishikawa, E. Nakamura, Origin of the slab component in arc lavas from across-arc variation of B and Pb isotopes. *Nature* **370**, 205–208 (1994).
55. T. Ishikawa, F. Tera, Two isotopically distinct fluid components involved in the Mariana arc: Evidence from Nb/B ratios and B, Sr, Nd, and Pb isotope systematics. *Geology* **27**, 83–86 (1999).
56. T. Ishikawa, F. Tera, T. Nakazawa, Boron isotope and trace element systematics of the three volcanic zones in the Kamchatka arc. *Geochim. Cosmochim. Acta* **65**, 4523–4537 (2001).
57. S. Tonarini, S. Agostini, C. Doglioni, F. Innocenti, P. Manetti, Evidence for serpentinite fluid in convergent margin systems: The example of El Salvador (Central America) arc lavas. *Geochem. Geophys. Geosyst.* **8**, Q09014 (2007).
58. T. J. Falloon, L. V. Danyushevsky, T. J. Crawford, R. Maas, J. D. Woodhead, S. M. Eggins, S. H. Bloomer, D. J. Wright, S. K. Zlobin, A. R. Stacey, Multiple mantle plume components involved in the petrogenesis of subduction-related lavas from the northern termination of the Tonga Arc and northern Lau Basin: Evidence from the geochemistry of arc and backarc submarine volcanics. *Geochem. Geophys. Geosyst.* **8**, Q09003 (2007).
59. N. S. Keller, R. J. Arculus, J. Hermann, S. Richards, Submarine back-arc lava with arc signature: Fonualei Spreading Center, northeast Lau Basin, Tonga. *J. Geophys. Res. Solid Earth* **113**, B08S07 (2008).
60. S. J. Turner, C. H. Langmuir, The global chemical systematics of arc front stratovolcanoes: Evaluating the role of crustal processes. *Earth Planet. Sci. Lett.* **422**, 182–193 (2015).
61. P. Ulmer, V. Trommsdorff, Serpentine stability to mantle depths and subduction-related magmatism. *Science* **268**, 858–861 (1995).
62. S. C. Penniston-Dorland, M. J. Kohn, C. E. Manning, The global range of subduction zone thermal structures from exhumed blueschists and eclogites: Rocks are hotter than models. *Earth Planet. Sci. Lett.* **428**, 243–254 (2015).
63. M. Scambelluri, O. Müntener, L. Ottolini, T. T. Pettke, R. Vannucci, The fate of B, Cl and Li in the subducted oceanic mantle and in the antigorite breakdown fluids. *Earth Planet. Sci. Lett.* **222**, 217–234 (2004).
64. S. J. Turner, C. H. Langmuir, What processes control the chemical compositions of arc front stratovolcanoes? *Geochem. Geophys. Geosyst.* **16**, 1865–1893 (2015).
65. V. J. M. Salters, A. Stracke, Composition of the depleted mantle. *Geochem. Geophys. Geosyst.* **5**, Q05B07 (2004).
66. A. Gale, C. A. Dalton, C. H. Langmuir, Y. Su, J.-G. Schilling, The mean composition of ocean ridge basalts. *Geochem. Geophys. Geosyst.* **14**, 489–518 (2013).
67. G. A. Gaetani, T. L. Grove, The influence of water on melting of mantle peridotite. *Contrib. Mineral. Petrol.* **131**, 323–346 (1998).
68. S. Schwartz, S. Guillot, B. Reynard, R. Lafay, B. Debret, C. Nicollet, P. Lanari, A. L. Auzende, Pressure–temperature estimates of the lizardite/antigorite transition in high pressure serpentinites. *Lithos* **178**, 197–210 (2013).
69. K. Kitada, N. Seama, T. Yamazaki, Y. Nogi, K. Suyehiro, Distinct regional differences in crustal thickness along the axis of the Mariana Trough, inferred from gravity anomalies. *Geochem. Geophys. Geosyst.* **7**, Q04011 (2006).
70. W. C. Crawford, J. A. Hildebrand, L. M. Dorman, S. C. Webb, D. A. Wiens, Tonga Ridge and Lau Basin crustal structure from seismic refraction data. *J. Geophys. Res. Solid Earth* **108**, 2195 (2003).
71. A. Beniest, W. P. Schellart, A geological map of the Scotia Sea area constrained by bathymetry, geological data, geophysical data and seismic tomography models from the deep mantle. *Earth Sci. Rev.* **210**, 103391 (2020).

Acknowledgments: We thank T. Plank, G. Abers, and M. Fortin for discussions. We are grateful to W. Leeman, M. Brounce, and K. Evans for thoughtful and constructive comments and to B. Schoene for efficient editorial handling. **Funding:** Y.Z. acknowledges funding from the National Science Foundation of China (91958213), the Chinese Academy of Sciences (XDB42020402), and the Shandong Provincial Natural Science Foundation, China (ZR2020QD068). This study was supported in part by the U.S. National Science Foundation NSF EAR 1826673 to E.G. and G.A.G. and OCE 1756349 to E.G. **Author contributions:** Y.Z. conceived the study and compiled the data. Y.Z. and E.G. analyzed data and wrote the manuscript. G.A.G. and F.K. contributed to the discussions. **Competing interests:** The authors declare that they have no competing interests. **Data and materials availability:** All data needed to evaluate the conclusions in the paper are present in the paper and/or the Supplementary Materials.

Submitted 30 April 2021
Accepted 7 October 2021
Published 26 November 2021
10.1126/sciadv.abj2515

Serpentinite-derived slab fluids control the oxidation state of the subarc mantle

Yuxiang ZhangEsteban GazelGlenn A. GaetaniFrieder Klein

Sci. Adv., 7 (48), eabj2515. • DOI: 10.1126/sciadv.abj2515